Earthquake size-frequency statistics in a forest-fire model of individual faults

Alejandro Tejedor*
Department of Theoretical Physics, University of Zaragoza, Pedro Cerbuna 12, 50009 Zaragoza, Spain

Javier B. Gómez†
Department of Earth Sciences, University of Zaragoza, Pedro Cerbuna 12, 50009 Zaragoza, Spain

Amalio F. Pacheco‡
Department of Theoretical Physics, University of Zaragoza and BIFI, Corona de Aragon 42, 50009 Zaragoza, Spain

(Received 11 March 2008; revised manuscript received 2 February 2009; published 3 April 2009)

The earthquake size-frequency distribution of individual seismic faults commonly differs from the Gutenberg-Richter law of regional seismicity by the presence of an excess of large earthquakes. Here we present a cellular automaton of the forest-fire model type that is able to reproduce several size-frequency distributions depending on the number and location of asperities on the fault plane. The model describes a fault plane as a two-dimensional array of cells where each cell can be either a normal site or a trigger site. Earthquakes start on trigger sites. Asperities appear as the dual entities of the trigger sites. We study the effect that the number and distribution of asperities (the dual of the set of trigger sites), the earthquake rate, and the aspect ratio of the fault have on the size-frequency distribution. Size-frequency distributions have been grouped into subcritical, critical, and supercritical, and the relationship between the model parameters and these three kinds of distributions is presented in the form of phase maps for each of the five asperity types tested. We also study the connection between the model parameters and the aperiodicity of the large earthquakes. For this purpose the concept of aperiodicity spectrum is introduced. The aperiodicity in the recurrence of the large earthquakes in a fault shows an interesting variability that can be potentially useful for prediction purposes.

DOI: 10.1103/PhysRevE.79.046102 PACS number(s): 64.60.av, 91.30.Dk

I. INTRODUCTION

If there is a well-established fact regarding regional seismicity it is the relationship between the magnitude of an earthquake and its frequency, known as the Gutenberg-Richter law [1]. This law is of the power-law type when magnitudes are expressed in terms of rupture area [2], $n \propto S^{-b}$, where n is the number of observed earthquakes with rupture area *greater than* S and b is the so-called b value, which is a "universal constant" in the range of 0.5–1.5, although $b \simeq 1$ is the commonest value [2–4]. The Gutenberg-Richter law [1] implies that earthquakes are, on a regional or world-wide scale, a self-similar phenomenon lacking a characteristic scale (but see Ref. [5] for a different point of view).

It is important to notice, however, that the Gutenberg-Richter law [1] is a property of *regional* or *global* seismicity, which appears when we average seismicity over big enough areas and long enough time intervals. In the last ten years, data have been collected to extract statistics on *individual* systems of earthquake faults [6]. Interestingly, it has been found that the distribution of earthquake magnitudes may vary substantially from one fault to another and that, in general, this type of size-frequency distribution is different from the Gutenberg-Richter law [1]. Many single faults or fault zones display power-law distributions for only *small* events (small compared with the maximum earthquake size a fault can support, given its area), which occur in the intervals between roughly quasiperiodic earthquakes of much larger size which rupture the entire fault. These large and quasiperiodic earthquakes are termed "characteristic" [7], and the resulting size-frequency distribution is referred to as characteristic earthquake distribution. It is important to note that the concept of characteristic earthquake is not universally accepted among seismologists [6,8,9].

In any case, due to the short period of instrumental earthquake records and the scarcity of paleoseismic studies [6,10–13], the statistics of naturally occurring earthquakes in single faults is poor. This fact justifies the development of "synthetic seismicity" models [14], in which long catalogs of events are generated by computer models of seismogenesis. Such models can be tuned by requiring that they reproduce to a reasonable degree what is known of the statistics of past seismicity and then used to make inferences about the behavior of seismicity using much longer and homogeneous catalogs of synthetic events.

Here, we propose a modification of an existing cellular automaton, the forest-fire model (FFM) [15,16], as an earthquake-cycle model. The link between cellular automata models and seismicity works by discretizing a fault as a one-dimensional (1D) or two-dimensional (2D) plane made up of a large number of patches. These models are usually nondeterministic and neglect the details of both elasticity and fault friction, substituting them by simple cellular automata rules. Despite their simplicity, they are able to reproduce various types of size-frequency statistics, including Gutenberg-Richter [1] and characteristic earthquake distributions [17–30].

The model presented here is (i) two dimensions, (ii) for a single fault, (iii) with a percolationlike stress-transfer mechanism, (iv) quasistatic, (v) with a static and dynamic friction

*atejedor@unizar.es
†jgomez@unizar.es
‡amalio@unizar.es

law with total stress drop, and (vi) dissipative. To this list we would add that our model is inspired by the concept of asperity, as it is the presence of particularly strong elements in the fault plane that actually controls its relaxation. In this paper we use the term asperity in the sense in Ref. [31], that is, in its macroscopic sense and not in the microscopic one as used in the Materials Science literature. Thus, an asperity is an area on a fault that is stuck and large earthquakes unload them. From this viewpoint, each fault has only one or few asperities [32,33]; it is common that these high-strength areas occupy boundary positions on the fault plane, but not necessarily so.

A one-dimensional version of this model has already been successfully used by the authors as a renewal model to reproduce important aspects of the seismic cycle of individual faults [34] and for prediction purposes [35,36]. This 1D version, also known as the minimalist model (MM) because of its simplicity, has the important advantage that several properties of the model can be analytically obtained by means of a Markovian chain approach [34], but it has the disadvantage of its low dimensionality and rigidity. The purposes of this paper are precisely to present the 2D version of the MM and to cast it in the already well-known framework of the FFM. For obvious reasons, we will call 2D-MM the two-dimensional version of the minimalist model although its relationship to the FFM cannot be forgotten.

Apart from the score of papers addressing the connection between heterogeneity and size-frequency statistics [37–45], the only previous work where the FFM has been directly linked to seismicity and the earthquake cycle is that of Newman and Turcotte [46]. Our model has in common with theirs—the use of a percolationlike stress-transfer mechanism—but differs in the way earthquakes are triggered: in Ref. [46] a characteristic earthquake is an infinite percolation cluster (i.e., a cluster of occupied sites spanning the lattice east–west or north–south). Because of this triggering mechanism, Newman-Turcotte [46] model is capable only of generating characteristic earthquakes, but no smaller ones in between. Our model generates earthquakes of all sizes, with a specific size-frequency distribution.

The paper is set out as follows. In Sec. II we present the model emphasizing its relationship to the forest-fire and minimalist models. Then, we graphically show the different types of asperity distributions and the type of two-dimensional grids that will be studied in the numerical simulations.

The results of the simulations are shown in Sec. III. First, we present the resulting size-frequency profiles and phase maps where the type of size-frequency distribution is related to the parameters of the model. Then, the recurrence probability of the large earthquakes is analyzed emphasizing the role of the aperiodicity as a useful compact index that evaluates the predictability of the large events. Section III concludes with a quantitative evaluation of the goodness of several prediction strategies.

Finally, in Sec. IV we come back to the nature of the model, its quantitative differences with the forest-fire model, discuss the results, and remark on the most relevant conclusions.

II. MODEL AND ITS SIMULATION

The FFM was introduced in Ref. [47] and modified in Ref. [15] to make it self-organized critical. The Drossel-Schwabl FFM (DS-FFM) [15] is defined in a hypercubic lattice of dimensionality $1<d<\infty$, although we will concentrate here on the $d=2$ case because of its immediate relevance to two-dimensional fault planes. The model can be boiled down to four cellular automaton rules [30]: (i) a green tree catches fire if any of its four nearest neighbors is burning; (ii) a burning tree turns into an empty site; (iii) at an empty site a green tree grows with a given probability p; and (iv) a green tree becomes a burning tree with a probability f even if none of its neighbors is burning (sparking probability). This fourth rule is the modification that Drossel and Schwabl [15] introduced in the original model. To make the implementation on a computer more feasible, a separation of time scales is imposed by assuming that the growth and spontaneous ignition cease as long as any trees are burning. In other words, the time scale of fires is much shorter than the time scale of tree growth and also than the time between sparks. In practical terms a realization of the DS-FFM chooses at random a site for ignition. If the site is occupied by a tree, this tree and all trees connected to it are instantaneously burnt down (i.e., the corresponding sites become empty); in the next time step, a tree is planted in a randomly chosen site of the lattice.

The DS-FFM can be easily "translated" into earthquake terminology: the 2-d lattice is the fault plane (horizontal size N and vertical size M); a site on the lattice is a small patch of the fault plane; a site with a tree becomes a loaded patch in the fault; and a fire is an earthquake. Time is measured by the planting of trees in the DS-FFM and by the addition of load (or stress) in our model. This slow stress buildup simulates the remote stress that plate motion adds to real faults. In the model it is added in discrete units (particles) that can be thought of as stress quanta [48]. What about the sparking probability? Here is where the concept of trigger site enters into the model. In the standard FFM any lattice site can be ignited if it is occupied by a tree. In the 2D-MM, and this is the key difference with the standard model, only specific lattice sites, the *trigger sites*, can be "ignited" and start an earthquake. So, we divide the lattice into two sets of sites: normal sites and trigger sites. Both types of sites can be unloaded (empty) or loaded (tree), but only trigger sites can start an earthquake. The earthquake starts at the very moment a trigger site becomes loaded. In other words, the more trigger sites the lattice has, the higher the sparking probability is. If a fraction f of sites is occupied by trigger sites then, on average, once every $1/f$ time steps an earthquake will be triggered. As in the standard model, the size of the resulting earthquake will depend on the number of occupied sites that belong to the same cluster as the ignited trigger site. After an earthquake, this cluster is emptied (unloaded) and in the next time step another particle is randomly deposited in the lattice. Clusters are identified and counted with the Hoshen-Kopelman algorithm [49].

It is important to stress that a trigger site is *not* an asperity. In a sense it is just its dual, as Fig. 1(a) shows. The relationship between trigger sites and asperities is based on the idea

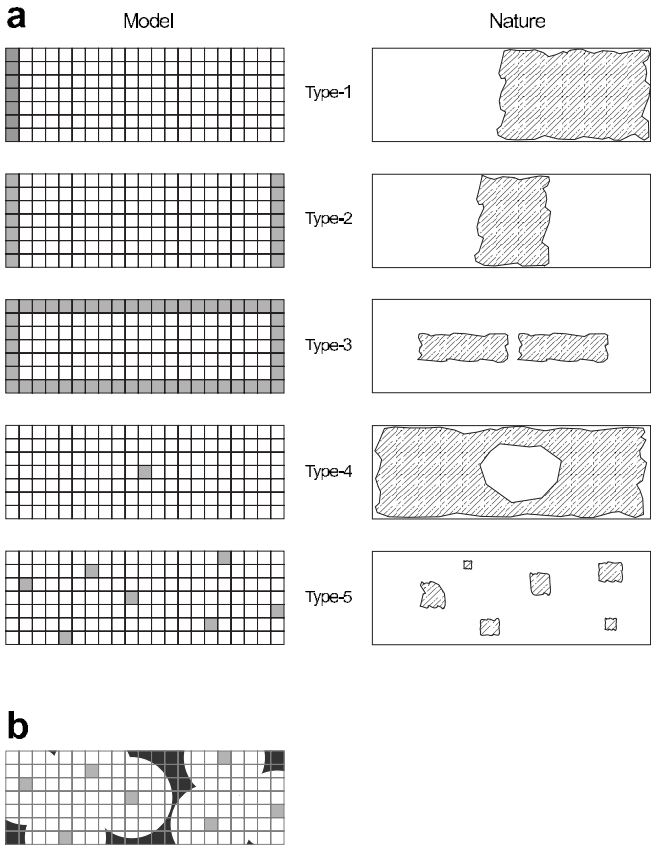

FIG. 1. (a) Types of trigger site distributions used in the simulations (left column) and their corresponding asperity maps on a fault plane (right column). From top to bottom, type 1: end asperity; type 2: central vertical asperity; type 3: central horizontal asperity; type 4: boundary asperities; and type 5: dispersed asperities. (b) Concept of zone of influence or catchment area. Each trigger site (light gray) is surrounded by an area (white circles) which is commonly unloaded upon failure. Regions of the lattice outside the catchment area of any trigger site (black) are the asperities. Here load accumulates and only when the lattice is highly loaded can it be depleted.

of a zone of influence or *catchment area* around each trigger site [Fig. 1(b)]. Sites close to a trigger site are commonly unloaded upon failure of the trigger site. On the other hand, sites far from trigger sites tend to accumulate load and are only unloaded when the total load on the lattice is high and the probability of finding a percolation path from a trigger site to a distant nontrigger site has increased. Thus, asperities are the set of sites outside the catchment area of any trigger site in the lattice [black areas in Fig. 1(b)]. The unloading of asperities gives rise to large earthquakes. The area occupied by asperities increases when the number of trigger sites decreases, making thus clear the dual relationship between asperities and trigger sites.

Figure 1(a) shows the five types of trigger site distributions that have been used in the simulations and the corresponding asperity maps on the fault plane. Type 1 is an end asperity and can be regarded as the main geometrical and/or mechanical heterogeneities that terminate a fault or divide it into segments. Type-2 and type-3 asperities are central asperities, i.e., particularly strong patches in the fault plane that control the way the fault relaxes. Type 4 is a boundary asperity, in a sense the opposite of a central asperity, where the weakest part of the fault is the central one. Finally, type-5 asperities are randomly distributed over the fault plane. This classification of asperity types does not intend to be exhaustive. It only includes extreme cases to better appreciate the influence of the number and distribution of asperities on the size-frequency statistics.

Because the sparking probability f depends on the number of trigger sites and the size of the lattice, it is not an independent parameter. For type-1 trigger sites $f=1/N$, for type-2 triggers, $f=2/N$, for type-3 triggers $f=[2(M+N-2)]/(MN)$, for type-4 triggers, $f=1/(MN)$, and for type-5 triggers, $f=1/N$ because we select M sites as trigger sites.

Apart from the number and distribution of asperities (which fixes the sparking probability f, i.e., the earthquake rate), the other parameters of the model are the size $N\times M$ of the lattice, N being the horizontal dimension and M being the vertical one, and the aspect ratio of the fault plane $r=N/M$. Only three of the four parameters r, f, N, and M are independent. The aspect ratio is important in real faults because it is related to the overall size of the fault plane, small faults being square (circular)—with $r\approx 1$—and big faults being rectangular—with $r>1$—due to the depth limit that the brittle-ductile transition imposes on the Earth crust (around 15 km for vertical strike-slip faults but can be more for subduction-type faults). Considering this depth limit and the range of surface fault trace lengths (from few kilometers for small earthquakes to 10^3 km for great earthquakes), a reasonable range of aspect ratios for real faults is $1<r<50$.

We want to explore the impact that the asperity distribution and the fault plane aspect ratio have on (i) the size-frequency distribution, (ii) the time between characteristic earthquakes, and (iii) the aperiodicity of the earthquake cycle. All three characteristics are important in assessing the predictability of the large earthquakes in the model.

III. RESULTS

A. Size-frequency distributions

To appreciate at a glance the type of size-frequency distributions that the model is able to produce, Fig. 2 shows several examples as a function of asperity type (upper panel), fault plane aspect ratio (middle panel), and fault size (lower panel). All three panels plot the noncumulative size-frequency distribution $P(k)$, where k is the size of an earthquake (i.e., the number of loaded patches connected to the trigger site). Figure 2(a) shows the effect of changing the type of asperity for a square system of size 50×50. Here we can already see the three main different types of size-frequency distributions [27]: supercritical (or characteristic earthquake type), critical (or Gutenberg-Richter type [1]), and subcritical. Type-1, 2, and 4 asperities produce supercritical size-frequency distributions, although the degree of supercriticality is not constant, increasing from type 2 to type 1 to type 4. Asperities of type 3 (boundary asperities) produce an almost-critical size-frequency distribution and type-5 asperities give a subcritical size-frequency distribution. In general terms, the degree of criticality is related to the size of the "bump" at the large-earthquake size end.

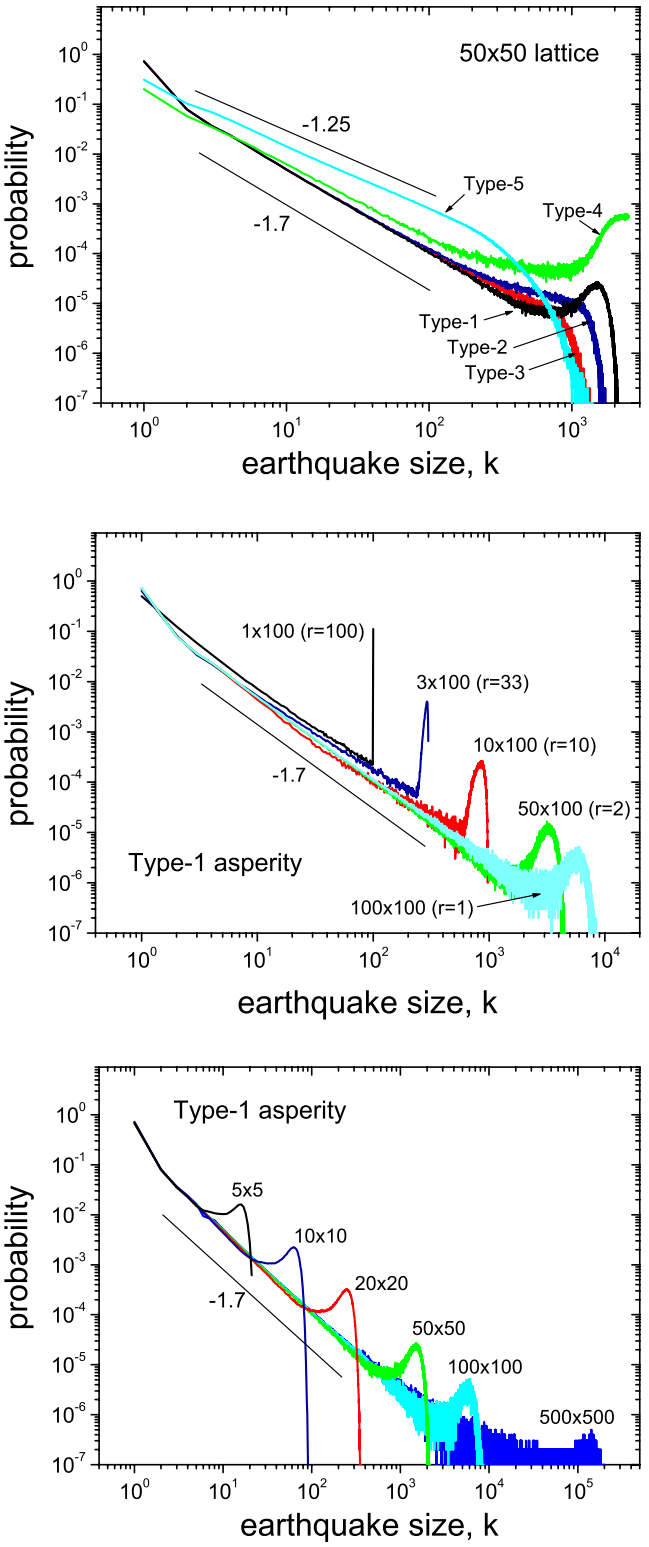

FIG. 2. (Color online) Size-frequency distribution for the 2D-MM as a function of type of asperity (upper panel), aspect ratio (middle panel), and system size (lower panel).

How the size-frequency distribution changes with the aspect ratio r for a type-1 asperity system which is shown in Fig. 2(b). The black curve is the size-frequency distribution for an $N=100$ one-dimensional MM [34], and the rest of the curves are for 2D systems with decreasing r, from 100 (elongated faults) to 1 (square faults). We see that the slope of the power-law part is the same for all aspect ratios and, more surprisingly, that the 1D and the 2D systems also have the same slope. An important difference between the 1D and the 2D versions of the MM is that in the 1D-MM a strict definition of a characteristic earthquake can be given, as only the biggest earthquakes ($k=100$ in the example) depart from the power-law curve. On the contrary, the 2D-MM has a broad range of large earthquakes that do not follow the power-law curve and which can thus be considered characteristic [7]. This will have important implications when discussing the predictability of the model. Notice, also, how the maximum that marks the characteristic size of the large earthquakes decreases as r decreases (f is constant and equal to 0.01 in all the curves) implying a dependence of the degree of criticality on the aspect ratio.

Finally, Fig. 2(c) depicts the change in size-frequency distribution as the size of a *square* system (i.e., $N=M$) is increased from $N=5$ to $N=500$. Here, r is constant and f varies from 0.2 (smallest lattice) to 0.002 (largest lattice). The basic observation is that the distribution is very robust, and little change can be appreciated as the size increases although the sparking probability decreases by 2 orders of magnitude. Although small, the change in the size-frequency distribution is apparent, with an increase in the degree of supercriticality as the sparking probability decreases [30].

This qualitative survey of the range of size-frequency distributions is insufficient to quantitatively relate the type of asperity to the parameters of the model. For that purpose, extensive numerical simulations have been carried out to reconstruct the phase space of the model. As already said, the model has four parameters, N, M, r, and f, although only three are independent. Cuts of the global phase space for each type of asperity are displayed in Fig. 3. Phase maps are shown with N in the horizontal axis and M in the vertical axis, together with r and f as isolines. Lines of constant aspect ratio are dashed, while lines of constant sparking probability are dotted. The type of size-frequency distribution is shown in yellow (light gray) for supercritical behavior, pale blue (middle gray) for critical behavior, and navy blue (dark gray) for subcritical behavior. Due to the difficulty in defining some transitional cases, two intermediate behaviors have been introduced for the transition from (pure) supercritical to (pure) critical behavior and for the transition from (pure) subcritical to (pure) critical behavior. We will now describe the behavior of the model for each asperity type.

1. Asperity type 1 (end asperity)

All the simulations carried out with trigger sites of the first type give a supercritical size-frequency relation (Fig. 3, first graph). Examples of specific size-frequency curves have already been given in Figs. 2(b) and 2(c). They clearly show the positive departure from the power law for large earthquakes that is the hallmark of supercritical behavior. The sparking probability (a proxy of earthquake rate) is independent of M, and so isolines are vertical (four are shown in the figure, from 0.01 on the left to 0.0025 on the right). Careful

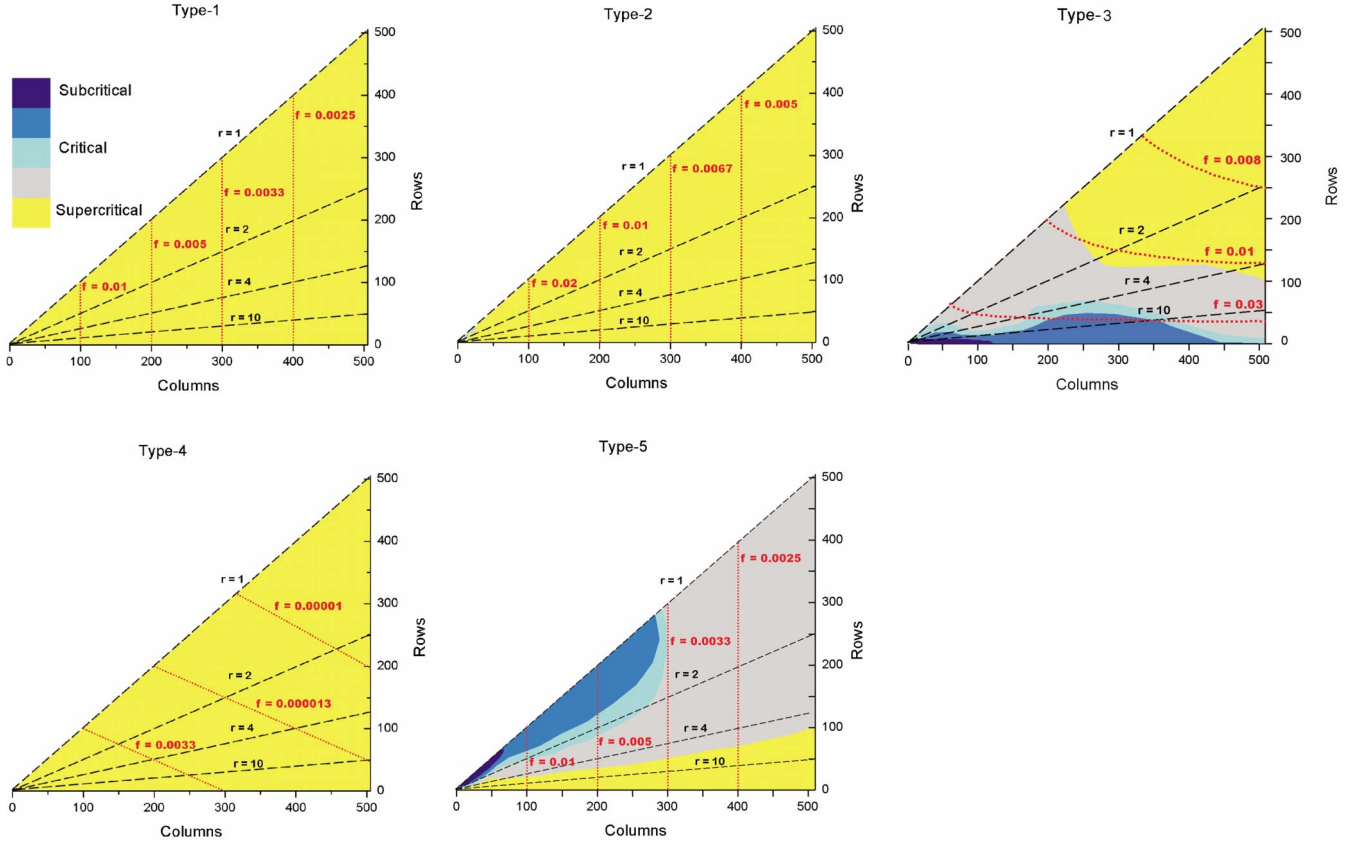

FIG. 3. (Color online) Phase maps for the five different asperity types. The four parameters of the model are explicitly shown in each graph. N increases from left to right and M from bottom to top. The other two parameters of the model are included as isolines (dashed lines for the aspect ratio r and dotted lines for the sparking probability f). The resulting type of size-frequency distribution is color coded in yellow (light gray) for supercritical behavior, cyan (middle gray) for critical behavior, and navy blue (dark gray) for subcritical behavior. Intermediate behaviors between supercritical and critical and between subcritical and critical are also included.

observation of specific size-frequency curves indicates that the degree of supercriticality varies more rapidly with the aspect ratio than with the sparking probability. The highest degree of supercriticality is connected in type-1 asperity simulations with elongated systems (large r) and small sparking probabilities. This is logical if we resort to the concept of catchment area introduced before [Fig. 1(b)]. If the aspect ratio is large (very elongated faults), trigger sites in a vertical edge are few and most of the lattice is outside their aggregated catchment area. Because of the elongated character of the lattice, few percolation paths are possible between trigger sites and the opposite end of the lattice, facilitating thus the storage of load in the asperities by simultaneously depleting the load in the catchment areas of the trigger sites. Few trigger sites also mean a low earthquake rate, favoring again the accumulation of load in the system and supercriticality.

2. Asperity type 2 (vertical central asperity)

This case has a unique large central asperity, elongated in the vertical direction, which is the dual of two sets of trigger sites occupying the two vertical edges of the lattice. The behavior of the system for asperities of the second type matches closely that of the previous case, although the degree of supercriticality is lower because the sparking probability is higher for the same N, M, and r. This is shown in the figure by the small area with critical behavior near the left corner of the triangle. For these simulations the positive excess of large earthquakes has disappeared. Obviously, the higher earthquake rate implied by the larger value of f precludes the complete filling of the lattice, inhibiting in this way the occurrence of system-wide earthquakes in this area of the phase space.

3. Asperity type 3 (horizontal central asperities)

Type-3 asperity systems have one or several central asperities elongated in the horizontal direction, far from all the edges of the fault plane as a consequence of the location of the trigger sites. The earthquake rate has increased again compared with type-1 and type-2 systems, so that f values are larger. This is clearly shown in Fig. 3, where almost half the area of the graph is below the $f=0.01$ isoline. Also, f isolines are now near horizontal, whereas in the two previous cases they are vertical, intersecting r isolines at high angles. This increase in the sparking probability gives rise to a richer variability of behavior, exhibiting the full range of size-frequency distributions, from subcritical for large-f, large-r lattices to supercritical for small-f, small-r lattices. The degree of supercriticality increases from the lower left corner to the upper right corner in the graph and depends both on f and

r. The smallest degree of supercriticality is found at the base of the triangle near its left corner. Here the earthquake rate is largest and so is the aspect ratio. A large aspect ratio tends to overlap the catchment areas of the upper and lower rows of trigger sites, making asperities very small or even nonexistent; this configuration inhibits the accumulation of load (favored also by the large-earthquake rate) and the system produces only small and medium earthquakes, but no large ones. This is the definition of subcritical behavior.

The upper right corner of the phase map has the opposite values of r and f, both being small. A square lattice maximizes the size of the central asperities and a small f minimizes the earthquake rate. Both effects facilitate the accumulation of load in the central part of the lattice and the production of system-wide earthquakes (supercritical behavior).

4. Asperity type 4 (boundary asperity)

Although this type of asperity distribution cannot be considered too realistic for surface-braking faults (the upper horizontal edge of these faults is always a free boundary) it can have some bearing on blind faults (those that do not reach the surface and are pinned at all four edges). Leaving aside the appropriateness of type-4 asperities in relation to real faults, they are interesting additions to the model, as they allow the exploration of very small values of f for a wide range of system sizes. Because of this, the sparking probability is very low compared with the other types of asperities. This sole characteristic makes the behavior universally supercritical, although supercriticality decreases toward the lower left corner of the graph. Isolines of f are straight lines with negative slope.

5. Asperity type 5 (distributed asperities)

This last type of asperity distribution differs from all the others in its stochastic nature. M trigger sites are randomly (but homogenously) located on the lattice. Homogeneously means that each row of the lattice has one and only one trigger site and no trigger site can share the same column. This assignment assures that all trigger sites are surrounded by nontrigger sites. Lines of constant f and r are identical to those of type-1 asperities, but the resulting phase map is completely different. Again, as was the case with type-3 asperities, the behavior is rich and size-frequency distributions of the three types are represented in different parts of the map. There is a clear dependence on r and f. Subcritical behavior is restricted to the small-r and large-f region, and supercritical behavior is found only in the lower part of the phase map, for large values of r (i.e., for elongated faults). Compared with type-3 systems, we see that now the subcritical region is restricted to square systems. This is a consequence of the way trigger sites are dispersed in the lattice (one per row and no two trigger sites in the same column). When the lattice is very elongated, few trigger sites are seeded and the probability is high of finding areas devoid of trigger sites (i.e., with asperities). On the other hand, when the lattice is square, many more trigger sites are seeded, and the probability of finding large asperities is consequently smaller; thus, the behavior of the system becomes less and less supercritical as r tends to 1 (for constant N).

B. Aperiodicity spectrum and interevent time distribution

A compact way of assessing the predictability of the large earthquakes in the 2D-MM model is by means of their aperiodicity α. The aperiodicity is a quantitative measure of the regularity of a time series. If μ is the average time between two consecutive characteristic earthquakes (i.e., the mean duration of the earthquake cycle) and σ is the standard deviation of the duration around the mean, then $\alpha=\sigma/\mu$. The aperiodicity is otherwise known as the coefficient of variation. Molchan [50] showed that the predictability of a nonperiodic sequence of events is determined by the coefficient of variation rather than the interevent time distribution itself.

We have computed the aperiodicity of the large earthquakes in the 2D-MM and an example of its behavior is shown in Fig. 4 as the thick gray line in the main plot. Because the definition of a characteristic earthquake in the 2D-MM is not as straightforward as in the 1D case [34], we have calculated, for completeness, the whole spectrum of aperiodicities, taking as the target of observation any earthquake bigger than k, from $k=1$ to $k=MN$. This is what the gray curve means in Fig. 4. The aperiodicity spectrum for the 2D-MM has several interesting properties: it starts ($k=1$) and ends ($k=MN$) at $\alpha\approx 1$; from $k=1$ it decreases to a minimum value ($\alpha\approx 0.3$ for a 10×100, type-1 asperity system); and then it starts increasing until reaching again $\alpha\approx 1$ for earthquakes close to the maximum allowable size. This behavior is similar for other sizes, aspect ratios, and asperity types and can thus be considered general.

Thus, we see how the aperiodicity spectrum evolves from pure Poissonian ($\alpha=1$) to quasiperiodic ($\alpha<1$) to $\alpha\approx 1$ again (but clearly non-Poissonian) as the minimum size of the target earthquakes changes from 1 to $M\times N$. In the same panel of Fig. 4 we have drawn the size-frequency distribution (black curve) to see how the increase in aperiodicity near the right-hand side of the plot relates to the deviation from the power law in the size-frequency distribution. Note that while the size-frequency curve $P(k)$ corresponds to individual (nonaccumulated) values of the size k, the curve of aperiodicities corresponds to accumulated ($\geq k$) values of its size.

The decrease in aperiodicity in the first part of the aperiodicity spectrum is easily explained. The time series of the 2D-MM can be considered as the superposition of two different processes: one process, the generation of events of any size, is random in time; the other, the generation of intermediate and large earthquakes, is quasiperiodic. So, when events of random origin are eliminated from a time series, what remains has, necessarily, a lower aperiodicity. This is why the aperiodicity decreases from 1 toward a minimum value. This minimum value depends on the asperity distribution, system size, and system aspect ratio. In particular, the regularity is enhanced as the aspect ratio r grows. It is clear that the elongated form favors the storing of many particles in the system (highly loaded fault) before one of the few trigger sites is hit, which will frustrate the formation of a big cluster of occupied sites. This low α value remains almost constant up to $k\geq k_3$, where $k_3=550$ (see the caption of Fig. 4). The reason for this lies in the fact that the middle-sized events $k_2<k<k_3$ have only a small impact on the complete range $k\geq k_2$, as they are scarce and their absence (when we

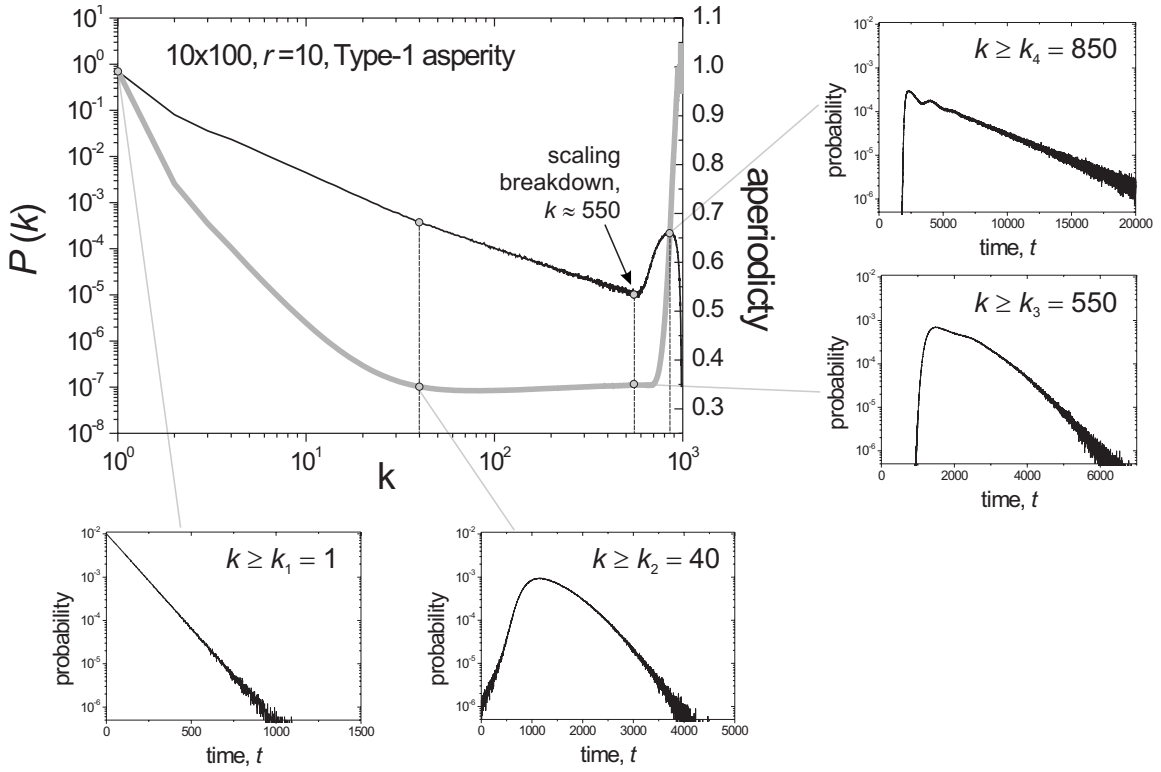

FIG. 4. Aperiodicity spectrum of a 10×100 system with a type-1 asperity (thick gray curve in main panel). The aperiodicity is plotted as a function of the minimum earthquake size k included in the time series. The main panel also shows the size-frequency distribution (black curve). The four smaller plots are interevent time distributions for specific points on the aperiodicity spectrum, $k\geq k_1=1$, $k\geq k_2=40$, $k\geq k_3=550$, and $k\geq k_4=850$. Point k_2 has been chosen inside the power-law section of the size-frequency distribution; point k_3 is located just where scaling breaks down (typically this occurs when more than half of the sites in the lattice participate in an earthquake), and point k_4 is located near the maximum on the characteristic earthquake hump. Time in these plots is dimensionless, measured in number of particles added to the system.

consider only the range of sizes $k\geq k_3$) is not so important from the aperiodicity point of view.

The reason for the increase in aperiodicity when considering only the final fraction of the largest earthquakes ($k>k_3$) is due to the fact that, in this model, the enhanced regularity (low α) corresponds to the *inclusive* consideration of all the large relaxations $k\geq k_3$ (that is, all the relaxations under the hump in the size-frequency distribution). Thus, when the target of observation does not take into account this unity but focuses only on sizes $k\geq k_4$, the regularity is lost and α grows. This is clearly seen in Fig. 5, where a particular although representative section of a time series coming from the 2D-MM is shown: the regularity in the occurrence of events is greater when all events above 550 are considered. If this lower limit of 550 is steadily increased, more and more large events (all belonging to the same group) are excluded from the time series and their aperiodicity increases. Near the maximum of the hump in the size-frequency distribution ($k_4=850$ in Fig. 5) the regularity of the sequence of events drops as the quasiperiodic process that generates these large earthquakes is split into its random components (each particular size).

The shape of the aperiodicity spectrum, as depicted in Fig. 4 is not unique to the 2D-MM. We have verified that the Abelian sandpile model [18,51,52] also has an aperiodicity spectrum which is qualitatively similar, with a high aperiodicity (close to one) both for all the events and only the largest ones and a minimum in between. The same is true for Burridge-Knopoff slider-block automata models [37,53].

Figure 4 also shows how the interevent time probability distribution changes with the definition of characteristic

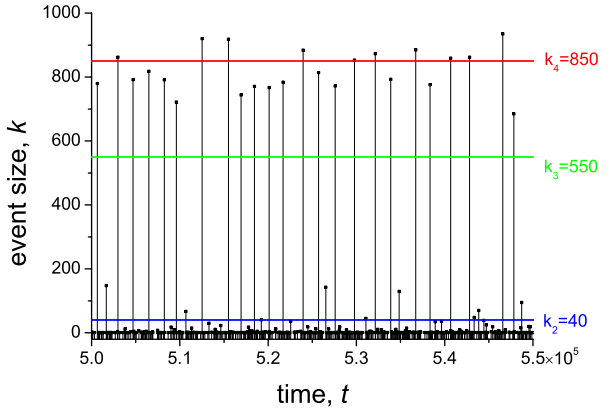

FIG. 5. (Color online) Time series for one realization of a 10×100 type-1 asperity system. 5×10^5 time units are shown (time is dimensionless, measured in number of particles added to the system). Each vertical line is an earthquake, whose height represents its size. Three sizes are highlighted by horizontal lines, $k_2=40$, $k_3=550$, and $k_4=850$.

earthquake. Time t is discrete and is measured in units of particles added since the last characteristic earthquake. Four interevent time probability distributions have been included, corresponding to four points on the aperiodicity spectrum ($k_1 \geq 1$, $k_2 \geq 40$, $k_3 \geq 550$, and $k_4 \geq 850$). The first point, $k_1 \geq 1$, includes all the events generated by the dynamics of the 2D-MM; the second point, $k_2 \geq 40$, is located where the aperiodicity levels off after the initial decrease; the third point, $k_3 \geq 550$, coincides with the deviations from the power law in the size-frequency distribution; and the fourth point, $k_4 \geq 850$, is at the summit of the hump that defines the characteristic earthquakes of the model.

The interevent time distribution for $k \geq 1$ is purely geometric, reflecting the Poissonian nature of the model when *all* earthquakes are included; the distribution for $k \geq 40$ has a maximum for $t > 0$ and faster than geometric decay for large times. The most important difference between this and the $k \geq 550$ distribution is that the former lacks a *stress shadow*. A stress shadow is the time period at the beginning of an earthquake cycle where the probability of having another great earthquake is zero and is a basic ingredient of all seismic faults. The $k \geq 550$ interevent time distribution corresponds to the end of the power-law section of the size-frequency distribution and is the most reasonable choice for the definition of characteristic earthquakes in the 2D-MM.

If we focus on just the largest earthquakes, $k \geq 850$, near the tip of the hump in the size-frequency distribution, we see that the interevent time distribution is not a exponential, although for longer times the decay is indeed exponential. Apart from the exponential tail, the interevent time distribution for the $k \geq 850$ case has a stress shadow for short time intervals and a maximum, followed by the exponential decay. Both elements of the interevent time distribution are important for the predictability of these earthquakes, as Sec. III C will clarify.

C. Forecasting

A convenient way to assess the predictability of a time series is by trying to forecast events (called *target events*) by declaring *alarms* at particular times. The aim is to declare alarms before all target events in order not to miss any, but to declare them *just* before the events in order to minimize the total alarm time. Many strategies can be devised to declare the alarms but there is a reference strategy to which all others can be compared [46,54,55]. This strategy consists of setting the alarm a fixed time interval (waiting time) after each target event and maintaining it until the occurrence of the event. If the following target event in the time series occurs before the alarm is raised, it is counted as a prediction error; if the following target event in the time series occurs after the alarm is raised, it is counted as a prediction success and the alarm is then canceled.

The fraction of errors f_e (number of missed events divided by the total number of events) and the fraction of alarm time f_a (total alarm time divided by the total duration of the time series) can be computed as a function of the waiting time t and the purpose is to find the optimum waiting time. This optimum waiting time depends on the relative importance that failing to predict an event has compared to keeping the alarm on. An objective function, called *loss function*, L, can be defined that incorporates this trade-off in each particular case. Here we will use the simplest of them, $L = f_e + f_a$, where failure to predict and a long alarm time are equally penalized. Obviously the aim is to find the waiting time $t = t^\star$ that minimizes $L(t)$. This minimum value is denoted by $L^\star = L(t^\star)$. The best way to graphically display this is by means of an error diagram, where the fraction of errors f_e runs along the horizontal axis and the fraction of alarm time f_a runs along the vertical axis (Fig. 6). Error diagrams were introduced in earthquake forecasting by Molchan [50] who contributed with rigorous mathematical analysis to the optimization of the earthquake prediction strategies. In an error diagram $L = 0$ means a perfect prediction (all the events have been predicted and the alarm was raised just before each event, so that $f_a \to 0$) and $L = 1$ means no prediction at all, either because we "predicted" all the events ($f_e = 0$) by keeping the alarm always on ($f_a = 1$) or because the alarm was always off ($f_a = 0$) and we missed all the events ($f_e = 1$).

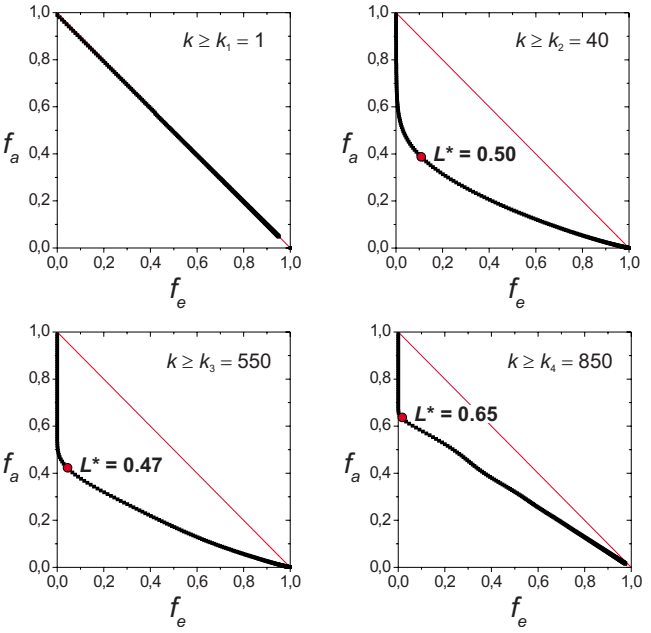

FIG. 6. (Color online) Error diagrams for the assessment of the predictability of large earthquakes in a 10×100 2D-MM system. The four panels show the outcome of the reference strategy for the four event sizes depicted in Fig. 4, i.e., for earthquakes with sizes $k \geq 1$, ≥ 40, ≥ 550, and ≥ 850. $L^\star$ is the minimum value of the loss function $L(t) = f_e(t) + f_a(t)$. Note that the best predictability corresponds to the case when all the earthquakes in the scaling breakdown section are taking into account (large hump in the size-frequency distribution in Fig. 4) and that this predictability is diminished when only part of the hump is chosen as the prediction target.

With these tools in hand, we return to the question raised at the beginning of the section about the predictability of the characteristic earthquakes in the 2D-MM model. Figure 6 shows the predictability of the same 10×100 2D-MM system whose aperiodicity spectrum and interevent time distributions were depicted in Fig. 4. Four error diagrams have been constructed with the reference strategy for events of sizes $k \geq 1$, $k \geq 40$, $k \geq 550$, and $k \geq 850$. Several observa-

tions are worth commenting on. For the $k \geq 1$ case, i.e., when all the earthquakes are taken into account, irrespective of their size, the interevent time distribution is an exponential distribution (see Fig. 4) and its error diagram for the reference forecasting strategy coincides with the $f_e + f_a = 1$ line, as it should be. In other words, the 2D-MM model is a realization of a Poisson process when all the events are included and the occurrence of earthquakes of any size is random in time.

Things get more interesting when small earthquakes are excluded and the focus is placed on the forecasting of larger events. When all earthquakes $k_2 \geq 40$ are included, the error diagram is no longer along the diagonal line. The minimum loss function is $L^\star = 0.50$, with $f_e \sim 0.11$ and $f_a \sim 0.39$. This diagram and the one for $k_3 \geq 550$ are quite similar, with a minimum loss function of $L^\star = 0.47$, slightly lower, and $f_e \sim 0.04$ (fewer events are missed, although the alarm time increases from 39% to 41%). This is compatible with the aperiodicity spectrum, as both sizes belong to the section of low aperiodicity (around 0.35) in Fig. 4. The main difference is in the width of the stress shadow region (zero in the k_2 case and different from zero in the k_3 case) which has its consequence in the error diagram in a reduction in the fraction of errors when the stress shadow is different from zero (only 4% of the events are missed compared with 11% in the former case). Finally, when a point is selected inside the characteristic earthquake hump ($k_4 \geq 850$), where the aperiodicity has again started to increase toward one, the error diagram has a minimum loss function considerably greater ($L^\star = 0.65$), meaning that the predictability of this fraction of characteristic earthquakes is lower than when all the characteristic earthquakes are taken as a group. These results agree with what we have seen in the aperiodicity spectrum in Fig. 4 and the qualitative explanation given in Sec. III C.

IV. DISCUSSION AND CONCLUSIONS

The 2D-MM tries to capture the basic functioning of an isolated seismic fault subjected to a long-term accumulation of stress (due to the plate motions) and a sudden release of stress by earthquakes. In this context, the separation of time scales is even more obvious than in the original DS-FFM because earthquakes have durations of seconds whereas times between earthquakes in the same fault are measured in terms of years or hundreds of years. The model is dissipative because a particle that hits a loaded site just disappears from the system. Time is discrete and ticks at the pace of the addition of particles, one per time step.

We have analyzed the 2D-MM in the light of the original FFM. The key difference with the DS-FFM is that ignition is limited to a subset of sites on the lattice, the trigger sites, and the topology of this subset controls the way the model behaves, as in real seismic faults [31,56]. Asperities are the dual of trigger sites and can be defined as the set of lattice sites outside the aggregated catchment area of all trigger sites. In particular, the model shows that faults can display both a Gutenberg-Richter [1] and a characteristic earthquake distribution depending on the number and location of asperities in the fault plane, as pointed out by several authors. [6,8,57]. The 2D-MM suggests that there is no specific distribution, and that it is the distribution of the asperities that controls the stress relaxation during the seismic cycle: one or few big compact asperities tend to give a characteristic earthquake distribution (i.e., type-1, type-2, and type-4 asperity systems), whereas small and/or distributed asperities tend to promote a Gutenberg-Richter [1] or subcritical one (type-3 and type-5 systems). This is compatible with what is known about real asperities in seismic faults [58–60].

The types of size-frequency distributions of the 2D-MM and DS-FFM are very similar but with an important difference: the slope of the power-law section. This slope reflects the distribution of cluster (fire, earthquake) sizes and is given by $kN(k) \approx k^{1-\tau}$, where $N(k)$ is the number of clusters of size k and τ is a critical exponent whose value is not yet well known for the DS-FFM but ranges from $\tau = 2.08$ [61] to $\tau = 2.15$ [62]. In the 2D-MM $\tau \approx 2.67$ for large lattices, well above the upper limit accepted for the DS-FFM. The change in critical exponent is clearly due to the topology of the subset of sites that can trigger avalanches. Precisely, the asperity of type 5 (Fig. 1) has been devised to simulate the way the DS-FFM relaxes and, as Fig. 2 demonstrates, the critical exponent changes from $\tau \approx 2.67$ to $\tau \approx 2.25$, approaching the value that characterizes the DS-FFM.

A useful element that has been introduced in this paper for the analysis of the predictability of discrete threshold systems is the *aperiodicity spectrum*. The aperiodicity spectrum quantifies the predictability of a time series as the definition of the events to be predicted changes. In other words, it summarizes the predictability of all the time series that can be constructed from the basic one when the minimum event size changes from 1 to the maximum allowable size ($N \times M$). The usefulness stems from the fact that the aperiodicity spectrum allows us to see important changes in the behavior of the "pruned" time series, changes that are related to the dynamics of the system. A similar plot in the context of spring-block models has also been used in Ref. [53].

Although the aperiodicity of a time series is by no means a rigorous proxy of its predictability, we have shown that a combination of the aperiodicity spectrum and error diagrams constructed for the reference strategy for specific points in the aperiodicity spectrum is a powerful graphical tool for the analysis of the predictability of the 2D-MM. Because we have observed that the behavior of the 2D-MM is more the rule than the exception as far as the aperiodicity spectrum is concerned (because the Abelian sandpile model has a qualitatively similar spectrum), it could be a useful tool for the analysis of the predictability of a whole group of threshold cellular automata [18,23,24,26,38,63]. A more in-depth analysis of the predictability of all these models is currently under way.

ACKNOWLEDGMENTS

This work was supported by the Spanish DGICYT (Project No. Fis 2005-06237). The authors thank Álvaro González for useful comments and discussions.

[1] B. Gutenberg and C. F. Richter, Bull. Seismol. Soc. Am. **34**, 185 (1944).
[2] H. Kanamori and D. L. Anderson, Bull. Seismol. Soc. Am. **65**, 1073 (1975).
[3] Y. Y. Kagan, Pure Appl. Geophys. **155**, 537 (1999).
[4] D. L. Turcotte, *Fractals and Chaos in Geology and Geophysics*, 2nd ed. (Cambridge University Press, Cambridge, 1999).
[5] L. Knopoff, Proc. Natl. Acad. Sci. U.S.A. **97**, 11880 (2000).
[6] S. G. Wesnousky, Bull. Seismol. Soc. Am. **84**, 1940 (1994).
[7] D. P. Schwartz and K. J. Coppersmith, J. Geophys. Res. **89**, 5681 (1984).
[8] Y. Y. Kagan, Bull. Seismol. Soc. Am. **86**, 274 (1996).
[9] S. G. Wesnousky, Bull. Seismol. Soc. Am. **86**, 286 (1996).
[10] K. Sieh, Proc. Natl. Acad. Sci. U.S.A. **93**, 3764 (1996).
[11] J. P. McCalpin and S. P. Nishenko, J. Geophys. Res. **101**, 6233 (1996).
[12] G. P. Biasi, R. J. Weldon, T. E. Fumal, and G. G. Seitz, Bull. Seismol. Soc. Am. **92**, 2761 (2002).
[13] R. D. Hartleb, J. F. Dolan, O. Kozacr, H. S. Akyuz, and S. S. Seitz, Bull. Seismol. Soc. Am. **118**, 823 (2006).
[14] R. Robinson and R. Benites, J. Geophys. Res. **100**, 18229 (1995).
[15] B. Drossel and F. Schwabl, Physica A **191**, 47 (1992).
[16] S. Clar, B. Drossel, and F. Schwabl, J. Phys.: Condens. Matter **8**, 6803 (1996).
[17] P. Bak, C. Tang, and K. Wiesenfeld, Phys. Rev. Lett. **59**, 381 (1987).
[18] P. Bak, C. Tang, and K. Wiesenfeld, Phys. Rev. A **38**, 364 (1988).
[19] P. Bak and C. Tang, J. Geophys. Res. **94**, 15635 (1989).
[20] K. Ito and M. Matsuzaki, J. Geophys. Res. **95**, 6853 (1990).
[21] M. Matsuzaki and H. Takayasu, J. Geophys. Res. **96**, 19925 (1991).
[22] H. Nakanishi, Phys. Rev. A **41**, 7086 (1990).
[23] K. Chen, P. Bak, and S. P. Obukhov, Phys. Rev. A **43**, 625 (1991).
[24] Z. Olami, Hans Jacob S. Feder, and K. Christensen, Phys. Rev. Lett. **68**, 1244 (1992).
[25] J. Lomnitz-Adler, L. Knopoff, and G. Martínez-Mekler, Phys. Rev. A **45**, 2211 (1992).
[26] B. Barriere and D. L. Turcotte, Phys. Rev. E **49**, 1151 (1994).
[27] I. Main, Rev. Geophys. **34**, 433 (1996).
[28] J. X. de Carvalho and C. P. C. Prado, Phys. Rev. Lett. **84**, 4006 (2000).
[29] K. Christensen, D. Hamon, H. J. Jensen, and S. Lise, Phys. Rev. Lett. **87**, 039801 (2001).
[30] S. Hergarten, *Self-Organized Criticality in Earth Systems* (Springer, New York, 2002).
[31] S. Das and K. Aki, J. Geophys. Res. **82**, 5658 (1977).
[32] W.-C. Chi, D. Dreger, and A. Kaverina, Bull. Seismol. Soc. Am. **91**, 1144 (2004).
[33] S. Santini, M. Dragoni, and G. Spada, Tectonophysics **367**, 219 (2003).
[34] M. Vázquez-Prada, A. González, J. B. Gómez, and A. F. Pacheco, Nonlinear Processes Geophys. **9**, 513 (2002).
[35] J. B. Gomez and A. F. Pacheco, Bull. Seismol. Soc. Am. **94**, 1960 (2004).
[36] A. González, J. B. Gómez, and A. F. Pacheco, J. Seismol. **10**, 131 (2006).
[37] R. Burridge and L. Knopoff, Bull. Seismol. Soc. Am. **57**, 341 (1967).
[38] Y. Ben-Zion and J. R. Rice, J. Geophys. Res. **100**, 12959 (1995).
[39] S. J. Steacy, J. McCloskey, C. J. Bean, and J. W. Ren, Geophys. Res. Lett. **23**, 383 (1996).
[40] Y. Ben-Zion, J. Geophys. Res. **101**, 5677 (1996).
[41] D. S. Fisher, K. Dahmen, S. Ramanathan, and Y. Ben-Zion, Phys. Rev. Lett. **78**, 4885 (1997).
[42] S. J. Steacy and J. McCloskey, Geophys. Res. Lett. **26**, 899 (1999).
[43] C. G. Sammis and S. W. Smith, Pure Appl. Geophys. **155**, 307 (1999).
[44] Y. Ben-Zion, K. Dahmen, V. Lyakhovsky, D. Ertas, and A. Agnon, Earth Planet. Sci. Lett. **172**, 11 (1999).
[45] S. Hainzl and G. Zöller, Physica A **294**, 67 (2001).
[46] W. I. Newman and D. L. Turcotte, Nonlinear Processes Geophys. **9**, 453 (1992).
[47] P. Bak, K. Chen, and C. Tang, Phys. Lett. A **147**, 297 (1990).
[48] S. Castellaro and F. Mulargia, Geophys. J. Int. **144**, 609 (2001).
[49] J. Hoshen and R. Kopelman, Phys. Rev. B **14**, 3438 (1976).
[50] G. M. Molchan, Pure Appl. Geophys. **149**, 233 (1997).
[51] D. Dhar, Phys. Rev. Lett. **64**, 1613 (1990).
[52] D. Dhar, Physica A **263**, 4 (1999).
[53] K. Christensen and Z. Olami, J. Geophys. Res., [Solid Earth Planets] **97**, 8792 (2002).
[54] M. Vázquez-Prada, A. González, J. B. Gómez, and A. F. Pacheco, Nonlinear Processes Geophys. **10**, 565 (2003).
[55] V. Keilis-Bork and A. Soloviev, *Nonlinear Dynamics of the Lithosphere and Earthquake Prediction* (Springer, New York, 2003).
[56] L. R. Johnson and R. M. Nadeau, Bull. Seismol. Soc. Am. **92**, 672 (2002).
[57] K. Dahmen, D. Ertas, and Y. Ben-Zion, Phys. Rev. E **58**, 1494 (1998).
[58] T. Lay and H. Kanamori, *Earthquake Prediction—An International Review* (American Geophysical Union, Washington, DC, 1981), pp. 579–592.
[59] C. H. Scholz, *The Mechanics of Earthquakes and Faulting* (Cambridge University Press, Cambridge, 1990).
[60] D. J. Wald, D. V. Helmberger, and T. H. Heaton, Bull. Seismol. Soc. Am. **81**, 8729 (1991).
[61] R. Pastor-Satorras and A. Vespignani, Phys. Rev. E **61**, 4854 (2000).
[62] P. Grassberger, J. Phys. A **26**, 2081 (1993).
[63] P. Bak and K. Sneppen, Phys. Rev. Lett. **71**, 4083 (1993).